Voronoi Diagrams in the Hilbert Metric

Auguste H. Gezalyan
Department of Computer Science, University of Maryland, College Park, MD, USA

David M. Mount
Department of Computer Science, University of Maryland, College Park, MD, USA

Abstract

The Hilbert metric is a distance function defined for points lying within a convex body. It generalizes the Cayley-Klein model of hyperbolic geometry to any convex set, and it has numerous applications in the analysis and processing of convex bodies. In this paper, we study the geometric and combinatorial properties of the Voronoi diagram of a set of point sites under the Hilbert metric. Given any m-sided convex polygon Ω in the plane, we present two randomized incremental algorithms and one deterministic algorithm. The first randomized algorithm and the deterministic algorithm compute the Voronoi diagram of a set of n point sites. The second randomized algorithm extends this to compute the Voronoi diagram of the set of n sites, each of which may be a point or a line segment. Our algorithms all run in expected time $O(mn \log n)$. The algorithms use $O(mn)$ storage, which matches the worst-case combinatorial complexity of the Voronoi diagram in the Hilbert metric.

2012 ACM Subject Classification Theory of computation → Computational geometry

Keywords and phrases Voronoi diagrams, Hilbert metric, convexity, randomized algorithms

Digital Object Identifier 10.4230/LIPIcs.SoCG.2023.35

Related Version *Full Version*: https://arxiv.org/abs/2112.03056

1 Introduction

The Hilbert metric was introduced by David Hilbert in 1895 [12]. Given a convex body Ω in d-dimensional space, it defines a distance function between any pair of points in the interior of Ω. (Definitions are presented in Section 2.1.) The Hilbert geometry has a number of natural properties. For example, straight line segments are geodesics. It generalizes the Cayley-Klein model of hyperbolic geometry (on Euclidean balls) to any convex body. It is also invariant under projective transformations. Hilbert geometry provides new insights into classical questions from convexity theory. It also provides new insights into the study of metric and differential geometries (such as Finsler geometries). An excellent resource on the Hilbert geometries is the handbook on Hilbert geometry by Papadopoulos and Troyanov [18].

Hilbert geometry is also relevant to the topic of convex approximation. Efficient approximations of convex bodies have been applied to a wide range of applications, including approximate nearest neighbor searching both in Euclidean space [6] and more general metrics [1], optimal construction of ε-kernels [4], solving the closest vector problem approximately [10, 11, 14, 19], computing approximating polytopes with low combinatorial complexity [3, 5]. These works all share one thing in common – they approximate a convex body by covering it with elements that behave much like metric balls. These covering elements go under various names: Macbeath regions, Macbeath ellipsoids, Dikin ellipsoids, and $(2, \varepsilon)$-covers. While these all behave like metric balls, the question is in what metric space? Vernicos and Walsh showed that these shapes are, up to a constant scaling factor, equivalent to Hilbert balls [2, 21].

In spite of its obvious appeals, there has been remarkably little work the design of algorithms in the Hilbert geometry on convex polygons and polytopes. Two notable exceptions are the work of Nielsen and Shao, which investigates properties and efficient construction of

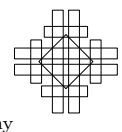

Hilbert balls in convex polygons [15], and Nielsen and Sun, which investigates clustering in Hilbert simplex geometry [16].

In this paper, we investigate perhaps the most fundamental computational questions one might ask about a metric geometry: How to construct the Voronoi diagram of a set of sites, points and/or line segments, in the plane? Given any convex polygon Ω bounded by m sides, we present two randomized algorithms and one deterministic algorithm for computing the Voronoi diagram of an n-element point set in the Hilbert metric induced by Ω. The first randomized algorithm works for point sites, while the second works for point sites and segment sites. Both run in $O(mn \log n)$ expected time. The deterministic algorithm works for point sites in $O(mn \log n)$ time and uses a divide-and-conquer approach. Due to space limitations the deterministic algorithm will be presented in the arXiv version of the paper. All the algorithms use $O(mn)$ space. We show that the worst-case combinatorial complexity of the Voronoi diagram is $\Theta(mn)$, so all the algorithms are worst-case optimal up to logarithmic factors.

2 Preliminaries

Throughout, let Ω denote a *convex body* in $\mathbb{R}^d$, that is, a compact, full-dimensional convex set. Let $\partial\Omega$ and $\text{int}(\Omega)$ denote its boundary and interior, respectively. Given points $p, q \in \mathbb{R}^d$, let $\|p - q\|$ denote the Euclidean distance between these points. Given two distinct points $p, q \in \Omega$, let $\chi(p, q)$ denote the *chord* defined as the intersection of the line passing through p and q with Ω.

2.1 Funk and Hilbert Metrics

Before defining the Hilbert metric, it will be convenient to define a simpler (asymmetric) distance function called the *Funk weak metric*.

▶ **Definition 1** (Funk weak metric)**.** *Given a convex body Ω in $\mathbb{R}^d$ and two distinct points $p, q \in \text{int}(\Omega)$, let y denote point where a ray shot from p to q intersects $\partial\Omega$. Define the* Funk weak metric *to be*

$$F_\Omega(p, q) \;=\; \ln \frac{\|p - y\|}{\|q - y\|},$$

and define $F_\Omega(p, p) = 0$ (see Figure 1(a)).

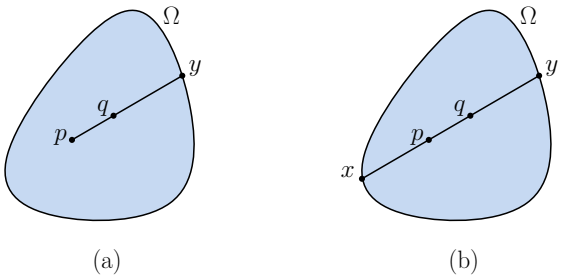

Figure 1 (a) The Funk weak metric and (b) the Hilbert metric.

Observe that in the limit as q approaches y along the chord $\chi(p, y)$ the Funk distance increases to $+\infty$, and thus, the boundary is infinitely far away from any interior point of Ω. The Funk weak metric is not symmetric, but it satisfies triangle inequality. Symmetrizing this yields a true metric, called the Hilbert metric [12].

▶ **Definition 2** (Hilbert metric). *Given a convex body Ω in $\mathbb{R}^d$ and two distinct points $p, q \in \text{int}(\Omega)$, let x and y denote endpoints of the chord $\chi(p, q)$, so that the points are in the order $\langle x, p, q, y\rangle$. Define the* Hilbert metric *to be*

$$d_\Omega(p, q) \;=\; \frac{F_\Omega(p, q) + F_\Omega(q, p)}{2} \;=\; \frac{1}{2} \ln \frac{\|p - y\|\|q - x\|}{\|q - y\|\|p - x\|},$$

and define $d_\Omega(p, p) = 0$ (see Figure 1(b)).

Hilbert showed that line segments are geodesics, and if q lies on the line segment between p and r, then $d_\Omega(p, q) + d_\Omega(q, r) = d_\Omega(p, r)$. Note however that generally there may be multiple shortest paths between two points, and hence geodesics need not be line segments (see, e.g., [7]). As in the Funk weak metric, the boundary of Ω is infinitely far away from any interior point. Observe that the quantity in the ln term in the definition is the cross ratio of $(p, q; y, x)$. It follows that the Hilbert metric is invariant under projective transformations. For further information, see the first chapters of the handbook on Hilbert geometry by Papadopoulos and Troyanov [18].

3 Hilbert Metric Balls

In this section we consider the properties of metric balls in the Hilbert metric. Given a convex body Ω in $\mathbb{R}^d$, $p \in \text{int}(\Omega)$, and $r \geq 0$, let us denote the *Hilbert ball* of radius r centered at p by

$$B_\Omega(p, r) \;=\; \{q \in \Omega \,:\, d_\Omega(q, p) \leq r\}.$$

We can extend the notion of distance to any nonempty set P in the natural way by taking the minimum distance to the set, that is, $d_\Omega(q, P) = \inf\{d_\Omega(q, p) \,:\, p \in P\}$. This allows us to talk about the Hilbert ball of other shapes, such as line segments. We will consider balls generated by both points and line segments.

3.1 Hilbert Balls of Points

Nielsen and Shao [15] provided a characterization of Hilbert balls when Ω is an m-sided convex polygon in $\mathbb{R}^2$, showing that the ball is a convex polygon bounded by at most $2m$ sides. We generalize their result to arbitrary convex polytopes in $\mathbb{R}^d$. This provides an alternative (and more elementary) proof that Hilbert balls are convex (also proved in [17,20]).

▶ **Lemma 3.** *Given any convex polygon Ω in $\mathbb{R}^2$ bounded by m sides, $p \in \text{int}(\Omega)$, and $r \geq 0$, the ball $B_\Omega(p, r)$ is a convex polygon bounded by at most $2m$ sides. It can be constructed in $O(m)$ time.*

Proof. For now, let us take Ω to be any convex body (not necessarily a polytope) in $\mathbb{R}^2$. Let $\mathbb{S}^1$ denote the unit sphere, that is the set of all unit vectors in $\mathbb{R}^2$. For each $u \in \mathbb{S}^1$, consider the ray emanating from p in direction u, and define $q_r(u) \in \Omega$ to be the (unique) point along this ray whose Hilbert distance from p is r. Clearly, the boundary of $B_\Omega(p, r)$ is just the set of points $q_r(u)$ over all $u \in \mathbb{S}^1$.

For any $u \in \mathbb{S}^1$, let $h(u)$ denote any support line of Ω at the point where the ray emanating from p in the direction u intersects the boundary of Ω (see Figure 2(a)). Define $h(-u)$ analogously for the ray emanating from p in the direction $-u$. Let $g(u)$ $(= g(-u))$ denote the point where $h(u)$ and $h(-u)$ intersect. (Through an infinitesimal perturbation of Ω, we may assume that $h(u)$ and $h(-u)$ are not parallel.) Let $b_r(u)$ denote the ray originating at $g(u)$ and passing through $q_r(u)$, and define $b_r(-u)$ analogously for $q_r(-u)$.

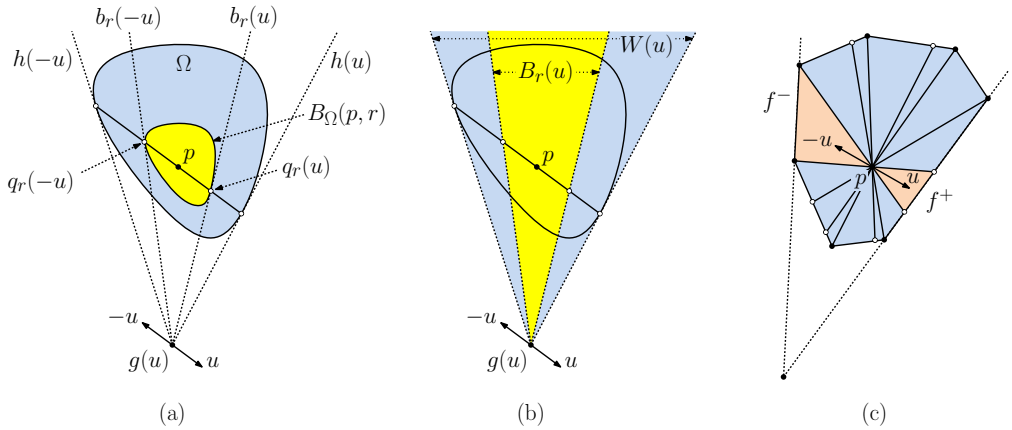

Figure 2 The Hilbert ball of a point p.

Let $W(u)$ denote the convex wedge whose apex is at $g(u)$ and is bounded by $h(u)$ and $h(-u)$ (see Figure 2(b)). It follows from basic properties of projective geometry that every line passing through p on this plane is cut by $h(u)$, $h(-u)$, $b_r(u)$, and p into four points that share the same cross ratio. This implies that every point on $b_r(u)$ is at Hilbert distance r from p with respect to $W(u)$. The same applies symmetrically to $b_r(-u)$, and therefore the sub-wedge of $W(u)$ bounded by $b_r(u)$ and $b_r(-u)$ is just the Hilbert ball of radius r centered at p for $W(u)$. (This was observed by Nielsen and Shao in their analysis of the two-dimensional case.) Let us call this sub-wedge $B_r(u)$ (shaded in yellow in Fig. 2(b)).

Note that $p \in \Omega \subseteq B_r(u)$, and therefore Hilbert distances from p in $B_r(u)$ are at least as large as they are in Ω. Therefore, for all $u \in \mathbb{S}^1$, $B_\Omega(p,r) \subseteq B_r(u)$, and hence

$$B_\Omega(p,r) \subseteq \bigcap\nolimits_{u\in\mathbb{S}^1} B_r(u).$$

On the other hand, by definition of $B_r(u)$, we know that $B_r(u)$ and $B_\Omega(p,r)$ both cover the exactly the same portion of the chord parallel to u passing through p. Since these chords cover all the boundary points of $B_\Omega(p,r)$, we have

$$B_\Omega(p,r) = \bigcap\nolimits_{u\in\mathbb{S}^1} B_r(u).$$

Clearly, $B_r(u)$ is the intersection of a (possibly infinite) set of convex wedges, and so it is also convex.

Suppose now that Ω is an m-sided convex polygon. We say that two sides f^+ and f^- form a *complementary pair* if there exists $u \in \mathbb{S}^1$ such that the rays emanating from p in the directions u and $-u$ hit $f+$ and f^-, respectively (see Figure 2(c)). We can partition the elements of $\mathbb{S}^1$ into equivalence classes according to the associated complementary pair. All the unit vectors u from any one equivalence class share the same support lines $h(u)$ and $h(-u)$, and therefore all of them contribute the same wedge $B_r(u)$ to $B_\Omega(p,r)$. By considering the chords $\chi(v,p)$ for each each of the m vertices of Ω, it follows directly that the number of complementary pairs is at most m. These chords partition Ω into at most m double wedges about p, each of which contributes two edges to the final ball, for a total of $2m$ sides.

The final Hilbert ball $B_\Omega(p,r)$ can be constructed in $O(m)$ time by observing that the sorted sequence of double wedges about p can be generated in linear time and then generating the two line segments bounding $B_r(u)$ within each double wedge (assuming a standard representation of Ω as a cyclic sequence of vertices). ◀

This result can be readily generalized to the higher dimensional case, but the worst-case number of bounding facets is quadratic in the number of facets. (Due to space limitations, the proof appears in the arXiv of the version of the paper.)

▶ **Lemma 4.** *Given any convex polytope Ω in $\mathbb{R}^d$ bounded by m facets, $p \in \text{int}(\Omega)$, and $r \geq 0$, $B_\Omega(p, r)$ is a convex polytope bounded by $O(m^2)$ facets.*

Given the characterization on Hilbert ball in $\Omega \in \mathbb{R}^2$, a natural question arises, how can we define Hilbert balls for points at infinity, that is, on $\partial\Omega$? Let q be a point in Ω, we define the Hilbert ball at $p \in \partial\Omega$ whose boundary passes through q to be limit of any sequence of Hilbert balls passing through q whose centers approach p. We show this limit is unique and yields a convex polygon with at most m sides.

▶ **Lemma 5.** *Given any convex polygon Ω in $\mathbb{R}^2$ bounded by m sides, $p \in \partial\Omega$, $q \in \text{int}(\Omega)$, there exists a unique ball, B, centered at p containing q on its boundary which is a convex polygon with at most m sides.*

Proof. Let us begin by considering an arbitrary sequence of Hilbert balls $\{B_n\}_{n\in\mathbb{N}}$ centered at points p_n such that $\{p_n\}_{n\in\mathbb{N}}$ converges to a point p on a side e of Ω (see Fig. 3(a)). Since our sequences converges to p there must be some $n_0 \in \mathbb{N}$ such that $\forall n \geq n_0$ in the sequence the wedges that contributes the boundary sides to $B_n, n \geq n_0$ all share the side e except the one made by the spokes through the vertices of e and p. Call this other wedge W with sides f^+ and f^-. It can be see that as $\{p_n\}_{n\geq n_0}$ approaches p, the measure of the region contributed by the wedge W vanishes to 0. Likewise, for any wedge W' between some e' and e, the portion of the boundary contributed between p_n and e vanishes in the limit. Hence we need only look at the boundaries contributed by the wedges between e and other sides of Ω.

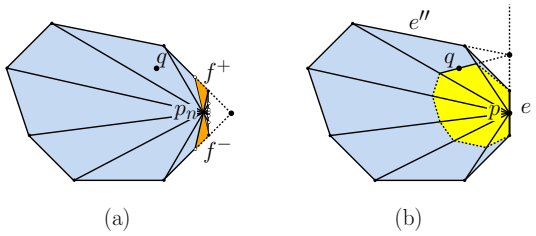

Figure 3 The Hilbert ball of a point p on $\partial\Omega$ through a point q.

To construct this boundary let q lie on the wedge between e and e'' from the perspective of p_n. By tracing the line through q to the apex of the wedge we are able to determine the boundary of an arbitrary p_n through q and a point on the boundaries of the neighboring wedges, from here we can walk along the wedges using the same process to complete the boundary. As p_n approaches p we can see that this converges to the unique polygonal boundary made by the same procedure applied to p. Since each wedge contributes one side to the boundary and there are $m-1$, paired with the edge e this gives the ball centered at p has at most m sides. ◀

3.2 Hilbert Balls of Lines and Line Segments

In this section we will describe the ball of radius r about an arbitrary line segment in Ω. Let us first consider the case of line ℓ that intersects Ω. Let $B_\Omega(\ell, r)$ denote the set of points of Ω that lie within Hilbert distance r of ℓ. We will consider just the 2-dimensional case, but the general case in $\mathbb{R}^d$ can be generated by considering the union of 2-dimensional slices generated by planes passing through ℓ. Given any point q in the interior of Ω, the following lemma characterizes the point of ℓ that is closest to q.

▶ **Lemma 6.** *Given any convex body Ω in $\mathbb{R}^2$ in general position and a line ℓ that intersects the interior of Ω, for any $q \in \text{int}(\Omega)$ that is not on ℓ, its closest point on ℓ is uniquely determined to be the point $p \in \ell$ such that there exist support lines from each of the endpoints of the chord $\chi(q,p)$ that intersect at a point lying on ℓ (see Fig. 4(a)).*

Proof. We begin by showing that, assuming general position, for any point $q \in \text{int}(\Omega)$, there exists a unique point p satisfying the desired properties. We first consider the simpler case where Ω is strictly convex, and we will generalize later. Let us also assume for the sake of illustration that ℓ is horizontal. Define t_0 and t_1 to be the leftmost and rightmost points of intersection of ℓ with Ω, respectively (see Fig. 4(b)).

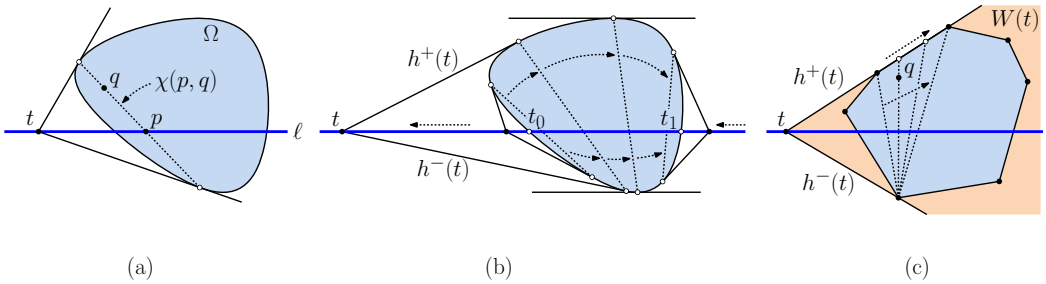

Figure 4 The closest point to q on line ℓ.

Consider a point t that moves continuously along $\ell \setminus \Omega$, which starts at t_0, moves to the left until reaching $x = -\infty$, then wraps around to $x = +\infty$, and finally moves to t_1. At each such point t, let $h^+(t)$ and $h^-(t)$ denote the two support lines of Ω that pass through t above and below ℓ, respectively. Since Ω is strictly convex, each pair of supporting lines defines a unique chord by joining the points where these support lines intersection $\partial\Omega$. It is a straightforward consequence of convexity that points where these support lines intersect $\partial\Omega$ move continuously and monotonically along both sides of the boundary of Ω from t_0 to t_1. Thus, every point of Ω lies on exactly one of these chords. Given point $q \in \text{int}(\Omega)$, the chord passing through q satisfies the conditions of the lemma. (Note that if Ω has vertices, multiple points t may generate the same chord. So even though the chord is unique, the associated supporting lines need not be.)

We can generalize to the case where Ω is not strictly convex. Suppose, for example, that it is an m-sided convex polygon. We may assume through an infinitesimal perturbation of ℓ that the linear extensions of any two edges of Ω do not intersect on ℓ. If we extend each edge of Ω until it intersects ℓ, we have m distinct points on $\ell \setminus \Omega$. It is no longer true that each point t generates a unique chord, but each point along the extended edge generates a chord in conjunction with the supporting vertex on the opposite side ℓ (see Fig. 4(c)). It follows from monotonicity that for any $q \in \text{int}(\Omega)$, exactly one of these chords passes through q.

Because the endpoints of each of these chords lies on opposite sides of ℓ, each chord intersects ℓ. We assert that the point p where this chord intersects ℓ is the unique closest point to q. To see why, consider the wedge $W(t)$ bounded by $h^+(t)$ and $h^-(t)$. Because the three lines ℓ, $h^+(t)$, and $h^-(t)$ are coincident at t, every line passing through q cuts these lines so that the cutting points have the same cross ratios. It follows that every point on ℓ is equidistant to q with respect to the Hilbert distance defined by $W(t)$. But (assuming general position) Ω intersects each such line through q along a strictly smaller subsegment, and hence the Hilbert distance between q and any point on ℓ other than p is strictly larger than $d_\Omega(q,p)$. Therefore, p is the unique closest point to q on ℓ. ◀

▶ **Lemma 7.** *Given any convex polygon Ω in $\mathbb{R}^2$ bounded by m sides, any line ℓ that intersects the interior of Ω, and $r \geq 0$, the Hilbert ball $B_\Omega(\ell, r)$ is a convex polygon bounded by at most $2m$ sides. Furthermore, this ball can be constructed in $O(m)$ time.*

Proof. Our proof is constructive. As in Lemma 6, let us assume that ℓ is horizontal. Consider the m points where the linear extensions of the edges of Ω intersect ℓ. We assume by general position that these points are distinct. As mentioned in the earlier proof, each of these points t generates two support lines $h^+(t)$ and $h^-(t)$ lying above and below ℓ, respectively. It also generates a continuous family of chords, by joining each point on the corresponding side $e(t)$ of Ω to the vertex of Ω through which the other support line passes (see Fig. 5(a) and (b)).

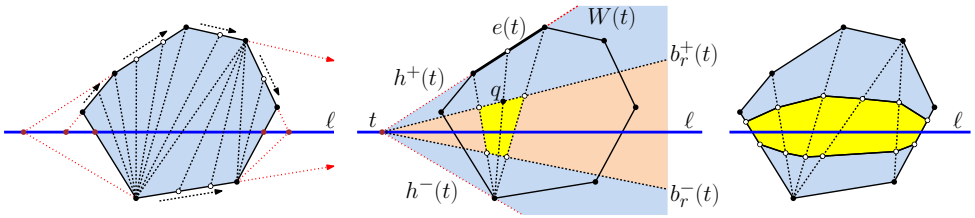

Figure 5 The Hilbert ball of a line ℓ.

Let $W(t)$ denote the double wedge bounded by $h^+(t)$ and $h^-(t)$. Given the radius r, we can draw a ray $b_r^+(t)$ emanating from t and passing above ℓ so that for every point q on $b_r^+(t)$, its Hilbert distance from ℓ with respect to $W(t)$ is r. As shown in Lemma 6, if q also lies on one of the chords generated by edge $e(t)$, then this is also true with respect to the Hilbert distance defined by Ω. Therefore, such a point q lies on the upper boundary of $B_\Omega(\ell, r)$ (see Fig. 5(b)). Analogously, we can find the ray $b_r^-(t)$, which generates the lower boundary of of $B_\Omega(\ell, r)$ for the chords generated by $e(t)$.

All that remains to complete the entire ball is to repeat this process for each of the m points t where the extensions of the sides of Ω intersect ℓ. The ball $B_\Omega(\ell, r)$ is clearly a simple polygon bounded by at most $2m$ sides. Convexity follows by observing that, due to the monotonicity of the points t along the line ℓ, the slopes of its sides along the upper boundary of the ball decrease monotonically and the slopes of sides along the lower boundary of the ball increase monotonically. ◀

Given two points $a, b \in \Omega$, the Hilbert ball of a line segment $\overline{ab}$ can be formed by first constructing the Hilbert ball for the line ℓ that passes through these points (see Fig. 6(a)), then cutting this ball through the chords of the line-ball construction passing through points a and b (see Fig. 6(b)), and finally filling in the missing ends with the portions of the Hilbert balls centered at the points a and b (see Fig. 6(c)).

▶ **Lemma 8.** *Given any convex polygon Ω in $\mathbb{R}^2$ bounded by m sides, any line segment $\overline{ab}$ for $a, b \in \Omega$, and $r \geq 0$, the Hilbert ball $B_\Omega(\overline{ab}, r)$ is a convex polygon bounded by at most $4m$ sides. Furthermore, this ball can be constructed in $O(m)$ time.*

4 Characterizing Voronoi Diagrams in the Hilbert Metric

Using our understanding of Hilbert balls we can characterize the Voronoi diagram of a set of point sites in the Hilbert metric. Throughout, let Ω denote a convex polygon in $\mathbb{R}^2$, and unless otherwise stated, distances will be in the Hilbert metric induced by Ω, which we

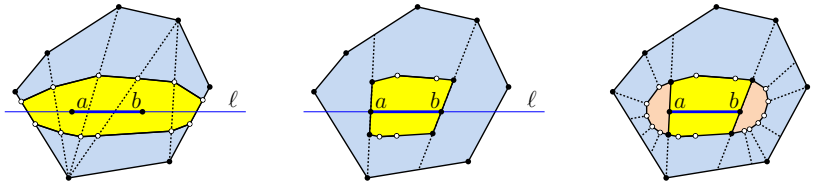

(a) (b) (c)

Figure 6 Three-step process for building the Hilbert ball of a line segment $\overline{ab}$.

denote by $d_\Omega(\cdot,\cdot)$ or simply $d(\cdot,\cdot)$, when Ω is clear. Let S denote a set of n points lying within the interior of Ω, which we call *sites*. For $p \in S$, define its *Voronoi cell* to be

$$V(p) \;=\; V_S(p) \;=\; \big\{q \in \Omega \,:\, d(q,p) \le d(q,p'),\, \forall p' \in S \setminus \{p\}\big\}.$$

Although points on the boundary of Ω are infinitely far from points in the interior of Ω, we can compare the relative distances between a fixed boundary point and two interior points by considering the limit as an interior point approaches this boundary point. The *Voronoi diagram* of S in the Hilbert metric induced by Ω, denoted $\mathrm{Vor}_\Omega(S)$, is the cell complex of Ω induced by the Voronoi cells $V(p)$ for all $p \in S$. We assume that the points of S are in general position, and in particular, the line passing through any pair of sites of S and the lines extending any two edges of Ω are not coincident at a common point (including all three being parallel). If this assumption does not hold, the bisectors separating Voronoi cells can widen into 2-dimensional regions.

Recall that a set $R \subseteq \mathbb{R}^d$ is a *star* (or is *star-shaped*) with respect to a point $p \in R$ if for each $q \in R$, the segment pq lies within R. We next show that Hilbert Voronoi cells are *stars*.

▶ **Lemma 9.** *Voronoi cells in the Hilbert Metric are stars with respect to their defining sites.*

Proof. If this were not the case, there would exist a site p and points $x, y \in \Omega$ such that $x \in V(p)$, $y \notin V(p)$, and y lies on the line segment px. By collinearity, $d(p,x) = d(p,y) + d(x,y)$. Letting q be the closest site to y, we have $d(q,y) < d(p,y)$ and $d(p,x) \le d(q,x)$. Combining these we have $d(q,x) + d(p,y) > d(q,y) + d(p,x)$, or equivalently $d(q,x) > d(q,y) + d(x,y)$. But this violates the triangle inequality, yielding a contradiction. ◀

4.1 Bisectors in the Hilbert Metric

Given two sites $p, p' \in \mathrm{int}(\Omega)$, we define their Hilbert bisector, denoted the (p,p')-*bisector*, to be $\{z \in \Omega : d_\Omega(z,p) = d_\Omega(z,p')\}$. We will explore the conditions for a point z to lie on the bisector. Let x and y denote the endpoints of the chord $\chi(z,p)$, and define x' and y' analogously for $\chi(z,p')$. Label these points in the order $\langle x,z,p,y\rangle$ and $\langle x',z,p',y'\rangle$ (see Figure 7(a)). Finally, let ℓ_x, ℓ_p, and ℓ_y denote the lines passing through the line segments xx', pp' and yy', respectively. If these three lines are coincident on some point q then by basic properties of projective geometry, the cross ratios $(z,p;y,x)$ and $(z,p';y',x')$ are equal. It follows that $d_\Omega(z,p) = d_\Omega(z,p')$, and hence z is on the bisector. If not, then the cross ratios are different and the Hilbert distances are different. Observe that as z approaches the boundary of Ω (on the same side of ℓ_p as ℓ_x), the points z, x, and x' converge on a common point on $\partial\Omega$, and ℓ_x approaches a support line for Ω at this point (see Figure 7(b)). Thus, we obtain the following characterization of bisector points.

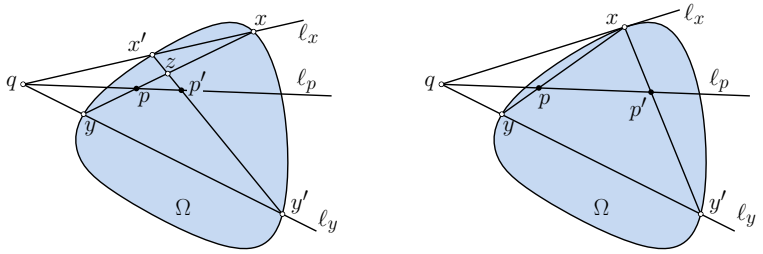

Figure 7 Conditions for a point z to lie on the Hilbert bisector between sites p and p'.

▶ **Lemma 10.** *Given a convex body Ω in $\mathbb{R}^2$, sites $p, p' \in \text{int}(\Omega)$ and any other point $z \in \text{int}(\Omega)$, z lies on the (p, p')-bisector if any only if lines ℓ_x, ℓ_p, and ℓ_y (defined above) are coincident. Further, a point $x \in \partial\Omega$ is on the Hilbert bisector if the coincidence holds when ℓ_x is any support line at x.*

When Ω is an m-sided convex polygon in $\mathbb{R}^2$, we can provide a more precise characterization of the bisectors. Given two sites $p, p' \in \text{int}(\Omega)$, we will show below that the (p, p')-bisector is a piecewise conic (see Lemma 14). Assuming this for now, we can characterize the breakpoints in this curve. Letting $\{v_1, \ldots, v_m\}$ denote the vertices of Ω, the $2m$ chords $\chi(v_i, p)$ subdivide Ω into $2m$ triangular regions, which we call p's *sectors* with respect to Ω (see Figure 8(a)).

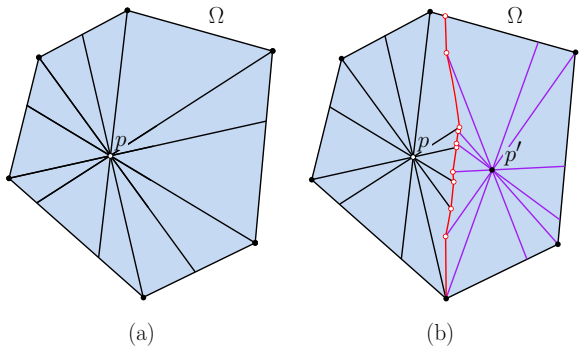

Figure 8 (a) The sectors of p with respect to Ω and (b) the Hilbert bisector (in red) between p and p'.

4.2 Bisector Segments and Combinatorial Complexity

For each point z on the (p, p')-bisector, let e and f denote the edges where the endpoints of chord $\chi(z, p)$ intersect $\partial\Omega$, and let e' and f' denote the corresponding edges of $\chi(z, p')$. Observe that the pair (e, f) is uniquely determined by the sector of p containing z, and the pair (e', f') is similarly determined by the sector of p' containing z. Therefore, the points of the (p, p')-bisector can be grouped into a discrete set of equivalence classes based on their sector memberships with respect to p and p' (see Figure 8(b)). We refer to these as *bisector segments*. Observe that by the star-shaped nature of Voronoi cells, as we travel along the bisector, we encounter the (up to $2m$) sectors of p in cyclic order (say clockwise as in the figure), and we visit (up to $2m$) the sectors of p' in the opposite cyclic order (counterclockwise). We will see below that, each bisector segment can be described by a

simple parametric function involving p, p', and the four edges defining the equivalence class. Star-shapedness implies that the bisector is simply connected. Combining the total number of sectors involved for each site, we have:

▶ **Lemma 11.** *Given an m-sided convex polygon Ω in $\mathbb{R}^2$ and sites $p, p' \in \text{int}(\Omega)$, the (p, p')-bisector is a simply connected piecewise curve consisting of at most $4m$ bisector segments.*

Given a set of n sites S in Ω, the Voronoi diagram consists of a collection of n Voronoi cells. The intersection of two cells $V(p)$ and $V(p')$ (if nonempty) is a portion of (p, p')-bisector, which we call a *Voronoi edge*. As shown in the above lemma, each such edge is composed of at most $4m = O(m)$ bisector segments. A cell's boundary may also contain a portion of the boundary of Ω. The intersection of two Voronoi edges (if nonempty) is a *Voronoi vertex*. Because the diagram is a planar graph, we have the following bounds by a straightforward application of Euler's formula.

▶ **Lemma 12.** *Given an m-sided convex polygon Ω in $\mathbb{R}^2$ and a set of n sites S in Ω, $\text{Vor}_\Omega(S)$ has n Voronoi cells, at most $3n$ Voronoi edges, and at most $2n$ Voronoi vertices. Each Voronoi edge consists of at most $4m$ bisector segments. Therefore, the entire diagram has total combinatorial complexity $O(mn)$. The average number of Voronoi edges per cell is $O(1)$, and the average number of bisector segments per cell is $O(m)$.*

The following lemma shows that the bound on the combinatorial complexity is tight in the worst case.

▶ **Lemma 13.** *For all sufficiently large m and n, there exists a convex polygon Ω' with m sides and a set S of n sites within Ω' such that $\text{Vor}_{\Omega'(S)}$ has combinatorial complexity $\Omega(mn)$. (Here we are using $\Omega(\cdot)$ in the asymptotic sense.)*

Proof. We start the construction with an axis parallel rectangle R that is slightly taller than wide, and the set S consists of n points positioned on a short horizontal line segment near the center of this rectangle (see Figure 9(a)). (This violates our general position assumptions, but the construction works if we perturb the sides of the rectangle.) Also, create a set of $m - 4$ points $V = \{v_1, \ldots, v_{m-4}\}$ along the left edge of R. We can adjust the spacing of points of V and S and the side lengths of R so that there exists a diamond shape (shaded in orange in the figure) so that for any point q in this region, the chord $\chi(v_i, q)$ intersects the boundary of R along its vertical sides. Observe that within the diamond, each consecutive pair of sites contributes an edge to the Voronoi diagram, which is easily verified to be a vertical line segment within the diamond.

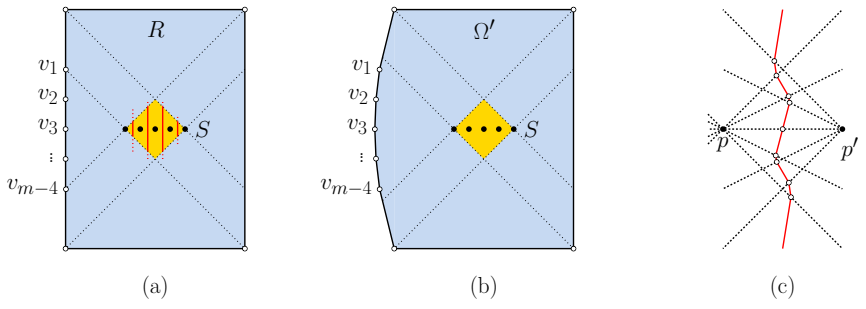

Figure 9 Proof of Lemma 13.

To form Ω', we bend the left side of the rectangle out infinitesimally (see Figure 9(b)) so the points of V become vertices of a convex polygon. The bending does not alter the shape of the Voronoi edges significantly, except to break each edge up into multiple arcs.

We assert that each consecutive pair of points $p, p' \in S$ contributes at least $m-4$ arcs to the Voronoi diagram. To see why, observe that there are $m-4$ sectors about p and p', and vertical line passing between p and p' intersects the boundaries between these sectors (see the red curve in Figure 9(c)). Due to the infinitesimal bending of the left side of R, each crossing produces a new segment on the bisector. Since there are $n-1$ consecutive pairs of sites, the total complexity of $\mathrm{Vor}_{\Omega'(S)}$ is at least $(m-4)(n-1) = \Omega(mn)$, as desired. ◀

4.3 Bisector Segments Structure

In this section we discuss the properties of bisectors in the Hilbert metric. We consider cases involving both points, lines, and combinations thereof. In particular, we prove that the bisectors are piece-wise conics.

First, we will characterize the local structure of a bisector between two point sites a and b with respect to Ω. Let us hypothesize that a point $q \in \mathrm{int}(\Omega)$ lies on the bisector between these sites (see Fig. 10(a)). Draw chords $\overline{aq}$ and $\overline{bq}$. Let us make the general-position assumption that these chords do not intersect vertices of Ω. Consider the two edges of Ω incident chord $\overline{aq}$, and let p_a be the point (possibly at infinity) where the linear extensions of these edges intersect (see Fig. 10(b)). Define p_b analogously for the chord $\overline{bq}$.

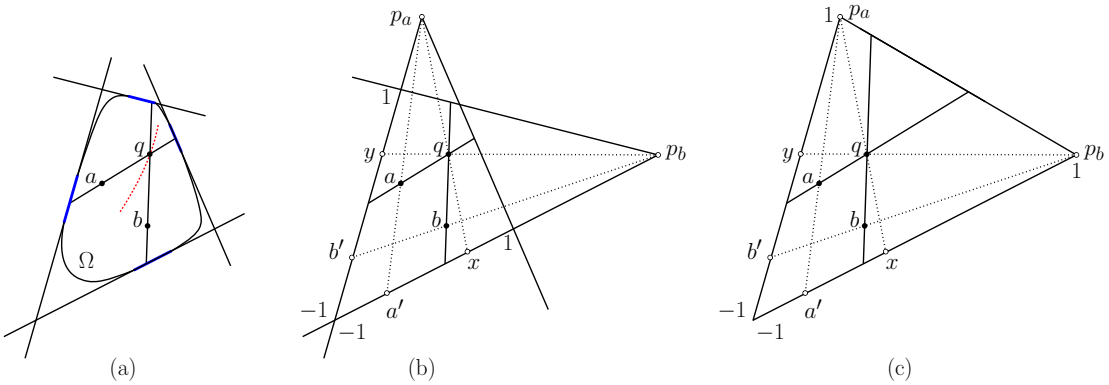

Figure 10 Segments of a point-point bisector.

If there are only two distinct edges involved (implying that $p_a = p_b$), the problem can be reduced to a simple 1-dimensional case by projection through the point where the extensions of the two edges meet. Otherwise, there are two wedges with apexes at the points p_a and p_b such that Ω is contained within their intersection. The shape resulting from the intersection of the two wedges may be a convex quadrilateral (as shown in Fig. 10(b)), but if two edges coincide, we obtain a triangle (see Fig. 10(c)). Also, this shape may be unbounded, which we treat as wrapping around the projective plane.

Shoot two rays originating at p_a passing through a and q, and let a' and x denote the respective points these rays hit on the opposite side of the quadrilateral (see Fig. 10(b)). Define b' and y analogously for rays originating at p_b through b. Let us parameterize points on these two edges so that -1 and 1 are the edge endpoints, and the points along the edge appear in the orders $\langle -1, a', x, 1\rangle$ and $\langle -1, b', y, 1\rangle$, respectively. We can now think of points $\{a', x, b', y\}$ as reals, where $-1 < a' \le x < 1$ and $-1 < b' \le y < 1$. (Due to space limitations, the proof appears in the arXiv version of the paper.)

▶ **Lemma 14.** *Given a convex polygon Ω and two sites $a, b \in \mathrm{int}(\Omega)$, the bisector between a and b in the Hilbert metric is a piecewise conic curve.*

Next, let us consider the case where a is a point site and $b = \overline{b_0 b_1}$ is a line segment, where $a, b_0, b_1 \in \Omega$. As before, we wish to characterize the set of points q lying on the Hilbert bisector between a and b with respect to Ω. Let ℓ_b denote the linear extension of this line segment.

Recall from Lemma 6 that the closest point on ℓ_b is uniquely determined to be the point b_q such that there exist support lines to Ω at the endpoints of the chord $\chi(q, b_q)$ that intersect at a point on ℓ_b (see Fig. 11(a)).

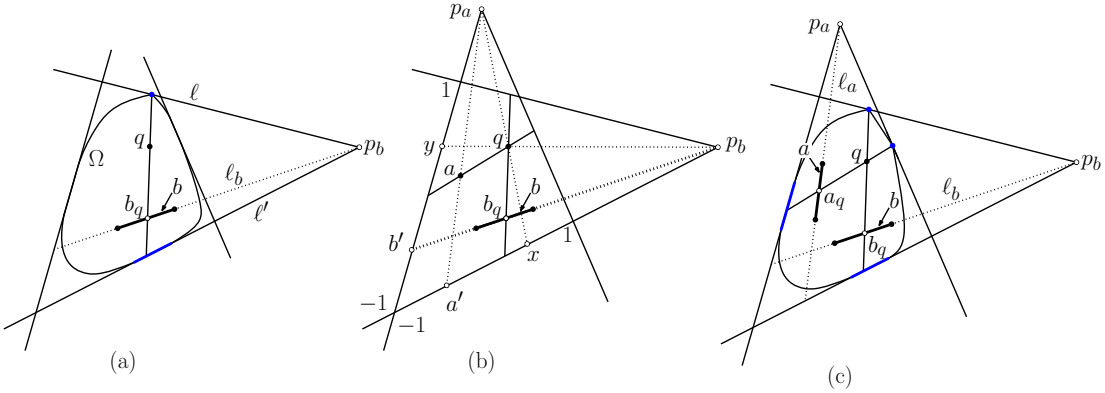

Figure 11 (a) Closest point on b to point q, (b) point-segment bisector, (c) segment-segment bisector.

Given the point p_b, we carry out the same construction as in the point-point bisector case, where the point p_a is defined exactly as before. We centrally project the points a and q through p_a until they hit the far side of the p_b-wedge, and symmetrically we centrally project the segment b and point q through p_b until they hit the far side of the p_a-wedge (see Fig. 11(b)). (Note that the entire segment b projects to the single point b'.) The values x and y, which determine curve containing the bisector, satisfy exactly the same conditions here as they do in the point-point case.

The segment-segment case is exactly analogous. Again, we find the point p_a through which the supporting lines pass, and obtain the same parameterization through central projections. The values x and y, which determine curve containing the bisector, satisfy exactly the same conditions here as they do in the point-point case.

It is interesting that unlike the Euclidean case, at a local level there is no fundamental difference between Hilbert bisectors in the point-point case and bisectors in the point-line or line-line cases. They are all conics, which may degenerate to lines in special configurations.

▶ **Lemma 15.** *Given a convex polygon Ω and two sites $a, b \in \text{int}(\Omega)$, either or both of which may be points or line segments, the bisector between a and b in the Hilbert metric is a piecewise conic curve.*

5 Randomized Incremental Algorithm

In this section we present two randomized incremental algorithms to compute the Hilbert Voronoi diagram of a set S of n sites. In both cases, the domain is an m-sided convex polygon Ω. First, we describe the algorithm in the case when S of n point sites. Second, we explain the changes when the sites are line segments. Both algorithms follow the structure of the randomized incremental algorithm for abstract Voronoi diagrams by Mehlhorn, Meiser, and Ó'Dúnlaing [13]. (A discussion on the relation of the Hilbert metric to abstract Voronoi diagrams can be found in the arXiv version of the paper.)

5.1 Point Sites

In this section we consider the construction of a Voronoi diagram for a set S of n point sites. The algorithm given in [13] starts by computing a bounding enclosure, but our body Ω serves that role. Let S be our set of sites. Consider an arbitrary iteration of the algorithm, and let R denote the set of sites already added to the diagram. To facilitate the constructing of our algorithm we maintain two data structures: $\mathrm{Vor}(R)$ the current Voronoi diagram of R as a cell complex, and $G(R)$ the *conflict graph* of R with respect to S (defined below).

$\mathrm{Vor}(R)$ may be stored in any standard data structure for planar subdivisions, such as a doubly connected edge list [9]. The vertices of $\mathrm{Vor}(R)$ are the Voronoi vertices and the edges are the bisectors connecting them. To facilitate efficient tracing of bisectors, we augment each Voronoi cell with *spokes*, that is, line segments emanating from each site in the diagram to the segment vertices of the bisectors forming its Voronoi cell (see Fig. 12).

The conflict graph $G(R)$ is defined as follows. Its vertices consist of the edges of $\mathrm{Vor}(R)$ together with the remaining sites $S \setminus R$. There is an edge between $e \in \mathrm{Vor}(R)$ and $p \in S \setminus R$ if and only if the addition of p would result in edge e either being removed or trimmed.

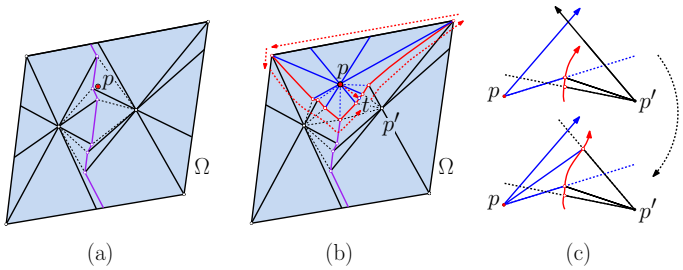

Figure 12 Inserting a new site in the randomized algorithm.

The algorithm randomly permutes the sites and inserts them one by one. The first two sites are inserted by brute force and the conflict graph is initialized based on the single bisector between these sites. Otherwise, let us assume that we have already inserted some subset R of sites and are now inserting the next site $p \in S \setminus R$. We need to (1) trace the boundary of p's Voronoi cell in $\mathrm{Vor}(R \cup \{p\})$ and (2) update the conflict graph. To trace a bisector between two sites we use the following method:

Let $V(p)$ denote the Voronoi cell of p after its insertion. We select any edge e that conflicts with p and we compute any point t on this edge that lies within p's Voronoi cell. We proceed to walk along the bisector, continuously maintaining the distances to the associated sites until reaching a point on the boundary of $V(p)$. Starting at this point, we proceed to trace the boundary of $V(p)$ in counterclockwise order about p (see Figure 12(b)). This involves two types of traces:

Bisector Trace: We are tracing the bisector between p and some existing site p' (see Figure 12(c)). We consider the sectors of p and p' containing the current portion of the (p, p')-bisector. By applying the parameterization from Lemma 14, we can trace the bisector until (1) we encounter the boundary of either sector, (2) we encounter the bisector between p' and another site, or (3) we encounter the boundary of Ω.
In the first case, we create a new segment vertex here, add spokes to this vertex, erase the extension of the sector edge (shown as a broken line in Figure 12(c)) and continue the tracing in the new sector. In the second case, we create a new Voronoi vertex, add spokes to this vertex from its three defining sites, and continue the trace along the new

bisector. In the third case, we insert two spokes joining the point where the bisector encounters the boundary to p and p', respectively. We then transition to the boundary trace described next.

Boundary Trace: We are tracing the Voronoi cell of p along the boundary of Ω. We walk along the boundary of Ω in counterclockwise order, considering each consecutive sector of the closest site p', prior to p's insertion. By applying the parameterization from Lemma 14, we determine whether the (p, p')-bisector intersects the boundary of Ω within the intersection of the current pair of sectors. If so, we identify this point on the $\partial\Omega$, add spokes to each of p and p', and then resume tracing along the (p, p')-bisector. Otherwise, we encounter one of the two sector boundaries, and we continue the tracing the next sector.

Along the way, we erase spokes from the current diagram, and/or introduce new spokes connected to p. When we return to our starting point, the insertion is completed.

While we are tracing the bisector for the new site, we can simultaneously update the conflict graph. Whenever we arrive at a new Voronoi vertex in the diagram, we construct a Hilbert ball at this point whose radius is the distance to the newly added site p (recall Lemma 3). This includes Voronoi vertices "at infinity", which arise whenever a bisector extends all the way to the boundary of Ω. Let p' and p'' be the two other sites of R that share this vertex. All the sites of $S \setminus R$ in this ball are added as conflict-graph neighbors of the two new Voronoi edges between p and p' and p and p''.

The algorithm given in [13] runs in $O(n \log n)$ expected time, under the *update assumption* of Clarkson and Shor [8], which states that the time to insert a new site p is proportional to the number of objects that conflict with regions that conflict with p. In our context, we need to add an additional factor of $O(m)$. First, this is needed because bisectors are no longer of constant complexity, but consist of $O(m)$ segments. Our algorithm processes each new segment in $O(1)$ time. Second, when updating the conflict graph, in order to determine which points conflict with the newly created edges, we need to construct a Hilbert ball at each newly created Voronoi vertex, and this takes time $O(m)$. The overall expected running time is thus larger by a factor of $O(m)$, implying the following.

▶ **Theorem 16.** *Given an m-sided convex polygon Ω in $\mathbb{R}^2$ and a set of n point sites S in Ω, the randomized incremental algorithm computes $\mathrm{Vor}_\Omega(S)$ in expected time $O(mn \log n)$ (where the expectation is over all possible insertion orders).*

5.2 Segment Sites

In this section, we present a sketch of the modifications necessary to generalize the algorithm from Section 5.1 to the case of line segments (due to space limitations, a more detailed account of the changes can be found in the arXiv version of the paper). Since the algorithm by Mehlhorn, Meiser, and Ó'Dúnlaing [13] is quite general, the approach applies here as well, but with a few changes.

First, we need to modify the notion of spokes to apply to segment objects. This is done by joining each bisector segment endpoint to its closest point on the segment (see Section 3.2). Second, the sector tracing process will be changed, but the complexity of the bisector is unaffected (see Lemma 15). Finally, the updating of the conflict graph is different, due to the fact that the circumcircles involved are now defined by combinations of point sets and segment sites.

Other than these changes, the algorithm and its analysis go through exactly as before. We suffer the same additional $O(m)$ in the running time due to complexity of Ω.

▶ **Theorem 17.** *Given an m-sided convex polygon Ω in $\mathbb{R}^2$ and a set of n point and line-segment sites S in Ω, the randomized incremental algorithm computes $\mathrm{Vor}_\Omega(S)$ in expected time $O(mn \log n)$ (where the expectation is over all possible insertion orders).*

References

1. Ahmed Abdelkader, Sunil Arya, Guilherme Dias da Fonseca, and David M. Mount. Approximate nearest neighbor searching with non-Euclidean and weighted distances. In *Proc. 30th Annu. ACM-SIAM Sympos. Discrete Algorithms*, pages 355–372, 2019. doi:10.1137/1.9781611975482.23.
2. Ahmed Abdelkader and David M. Mount. Economical Delone sets for approximating convex bodies. In *Proc. 16th Scand. Workshop Algorithm Theory*, pages 4:1–4:12, 2018.
3. Rahul Arya, Sunil Arya, Guilherme Dias da Fonseca, and David M. Mount. Optimal bound on the combinatorial complexity of approximating polytopes. *ACM Trans. Algorithms*, 18:1–29, 2022. doi:10.1145/3559106.
4. Sunil Arya, Guilherme Dias da Fonseca, and David M. Mount. Near-optimal ε-kernel construction and related problems. In *Proc. 33rd Internat. Sympos. Comput. Geom.*, pages 10:1–15, 2017.
5. Sunil Arya, Guilherme Dias da Fonseca, and David M. Mount. On the combinatorial complexity of approximating polytopes. *Discrete Comput. Geom.*, 58(4):849–870, 2017. doi:10.1007/s00454-016-9856-5.
6. Sunil Arya, Guilherme Dias da Fonseca, and David M. Mount. Optimal approximate polytope membership. In *Proc. 28th Annu. ACM-SIAM Sympos. Discrete Algorithms*, pages 270–288, 2017.
7. Herbert Busemann. *The Geometry of Geodesics*. Academic Press, 1955.
8. Kenneth L. Clarkson and Peter W. Shor. Applications of random sampling in computational geometry, ii. *Discrete Comput. Geom.*, 4:387–421, 1989. doi:10.1007/BF02187740.
9. Mark de Berg, Otfried Cheong, Marc van Kreveld, and Mark Overmars. *Computational Geometry: Algorithms and Applications*. Springer, 3rd edition, 2010.
10. Friedrich Eisenbrand, Nicolai Hähnle, and Martin Niemeier. Covering cubes and the closest vector problem. In *Proc. 27th Annu. Sympos. Comput. Geom.*, pages 417–423, 2011.
11. Friedrich Eisenbrand and Moritz Venzin. Approximate CVPs in time $2^{0.802n}$. *J. Comput. Sys. Sci.*, 124:129–139, 2021. doi:10.1016/j.jcss.2021.09.006.
12. D. Hilbert. Ueber die gerade Linie als kürzeste Verbindung zweier Punkte. *Math. Annalen*, 46:91–96, 1895.
13. K. Mehlhorn, St. Meiser, and C. Ó'Dúnlaing. On the construction of abstract Voronoi diagrams. *Discrete Comput. Geom.*, 6:211–224, 1991. doi:10.1007/BF02574686.
14. Márton Naszódi and Moritz Venzin. Covering convex bodies and the closest vector problem. *Discrete Comput. Geom.*, 67:1191–1210, 2022. doi:10.1007/s00454-022-00392-x.
15. Frank Nielsen and Laetitia Shao. On balls in a Hilbert polygonal geometry (multimedia contribution). In *Proc. 33rd Internat. Sympos. Comput. Geom.*, volume 77 of *Leibniz International Proceedings in Informatics (LIPIcs)*, pages 67:1–67:4. Schloss Dagstuhl–Leibniz-Zentrum für Informatik, 2017. doi:10.4230/LIPIcs.SoCG.2017.67.
16. Frank Nielsen and Ke Sun. Clustering in Hilbert's projective geometry: The case studies of the probability simplex and the elliptope of correlation matrices. In Frank Nielsen, editor, *Geometric Structures of Information*, pages 297–331. Springer Internat. Pub., 2019. doi:10.1007/978-3-030-02520-5_11.
17. Athanase Papadopoulos and Marc Troyanov. From Funk to Hilbert geometry. In *Handbook of Hilbert geometry*, volume 22 of *IRMA Lectures in Mathematics and Theoretical Physics*, pages 33–68. European Mathematical Society Publishing House, 2014. doi:10.4171/147-1/2.

18 Athanase Papadopoulos and Marc Troyanov. *Handbook of Hilbert geometry*, volume 22 of *IRMA Lectures in Mathematics and Theoretical Physics*. European Mathematical Society Publishing House, 2014. doi:10.4171/147.

19 Thomas Rothvoss and Moritz Venzin. Approximate CVP in time $2^{0.802n}$ – Now in any norm! In *Proc. 23rd Internat. Conf. on Integ. Prog. and Comb. Opt. (IPCO 2022)*, pages 440–453, 2022. doi:10.1007/978-3-031-06901-7_33.

20 Marc Troyanov. Funk and Hilbert geometries from the Finslerian viewpoint. In *Handbook of Hilbert geometry*, volume 22 of *IRMA Lectures in Mathematics and Theoretical Physics*, pages 69–110. European Mathematical Society Publishing House, 2014. doi:10.4171/147-1/3.

21 Constantin Vernicos and Cormac Walsh. Flag-approximability of convex bodies and volume growth of Hilbert geometries. HAL Archive (hal-01423693i), 2016. URL: https://hal.archives-ouvertes.fr/hal-01423693.